Input Impedance of an Aperture over a Lossy Half-Space: Application to On-Body Antenna Performance at 60 GHz

Solofo Razafimahatratra[1], [*], Julien Sarrazin[1], Guido Valerio[1], François Sarrazin[2], Massimiliano Casaletti[1], Philippe De Doncker[3], and Aziz Benlarbi-Delaï[1]

Abstract—This paper presents a theoretical approach to compare the performance of a directive and a quasi-omnidirectional on-body antennas. Two canonical antennas, namely, a dipole and a rectangular aperture, are considered in the 60 GHz band. We first demonstrate that for this on-body configuration, the classically-defined far-field antenna gain depends on the observation distance. Consequently, we derive results in terms of radiation efficiency and link budget. To do so, the antenna input impedance computation is a preliminary step to normalize the input power to allow a fair comparison between the two antennas. The impedance over a lossy half-plane of an aperture illuminated by a TE_{10} mode normally polarized is therefore derived into a convenient easy-to-compute formulation, which to authors' best knowledge, is not available in the literature. In terms of link budget, it is obtained that the received power due to an aperture is generally higher than the one due to the dipole in the main lobe direction. A constant difference is observed along the distance, and this difference increases with the aperture width for antennas touching the body. Besides, it is shown that the standard aperture waveguide WR15 exhibits a slightly higher efficiency than a vertical dipole with the same vertical size when being placed at a distance less than 3 mm (i.e., 0.6λ) from the body phantom surface. Above this distance, the dipole and the aperture exhibit similar efficiency in the order of 60%.

1. INTRODUCTION

Body Area Network (BAN) is a fundamental technology for remote vital data sign monitoring. It is becoming ubiquitous since wearable communicating devices are more and more used for different applications such as wellbeing monitoring, sport, multimedia entertainment [1, 2], virtual reality, and assistance for people with disabilities [3]. BANs have to ensure reliable communications while offering a sufficient autonomy for users. Energy is indeed an issue in BANs since the room for the battery is often limited. Wireless communications usually consume a large part of the power available in small sensors [4]. Therefore, it is important to understand the link budget as well as the antennas radiation behavior when wireless communications take place on the human body (or in the body vicinity).

To do so, channel modeling based on measurements is usually performed. However, as stated in [5], a BAN channel model is antenna-specific unless antenna de-embedding is performed. On-body antenna de-embedding is a real challenge due to the strong coupling between the body and the antenna. This problem was addressed in simulation in [6] where an arbitrary distance has been chosen to separate the antenna from the channel. The antenna is simulated with the close-surrounding human body part, being typically small, using FDTD (Finite Difference Time Domain) simulation. Equivalent small electric dipoles are then determined on the surface of a cuboid which enables to couple it to an analytical

* Corresponding author: Solofo Razafimahatratra (solofo.razafimahatratra1@etu.upmc.fr).

[1] Laboratoire d'Electronique et Electromagnétisme, Sorbonne Universités, UPMC Univ Paris 06, UR2, L2E, F-75005, France. [2] ESYCOM (EA 2552), UPEMLV, ESIEE-Paris, CNAM, F-77454 Marne-la-Vallée, France. [3] Wireless Comm. Group, OPERA Dpt., Université libre de Bruxelles, Belgique.

channel, modeled by Bannister formulations. Using a similar approach but based on Spherical Wave Functions, authors in [7] extended the concept to measurements under some simplification assumptions. In that way, works in [6] and [7] enable to compare the performance of different specific antennas for a given channel. Regarding the antenna's intrinsic properties when located on the human body, several studies in the literature investigated the radiation efficiency compared with the efficiency when located in free-space. This degradation was reported in [8] at about 20% for two dual-band textile antennas (2.45 GHz and 5.2 GHz) embedded on a real person inside a reverberation chamber. In [9], the efficiency of a wearable textile patch antenna resonating at 2.4 GHz has been measured in an anechoic chamber at 29%, when being placed in direct contact to a phantom, and to 51%, with an 8 mm-spacing distance with the phantom. Finally, it is reported in simulation in [10] that a directional slot antenna achieves a higher efficiency than an Omni-directional monopole antenna on-body between 3 GHz and 6 GHz. All these studies do consider specific antenna topologies on a specific human body and it is therefore difficult to draw general conclusions. This is why an analytical approach was undertaken in our former study [11] to define on-body radiation efficiency and its dependence on frequency for a vertical dipole. However, the question of whether it is better to use an antenna with low or high directivity has not been investigated from an analytical point of view.

Consequently, this paper proposes a theoretical approach to compare two radiating antennas on the body in terms of link budget performance and radiation efficiency. The study considers two canonical antennas, namely a dipole and a rectangular aperture, normally polarized on the surface of a planar phantom with the same dielectric properties than the skin. Due to the recent interest in the license-free 60 GHz band for BANs [12–15], obtained results will be illustrated at this frequency. To compare the power radiated by these two antennas, it is necessary to determine the accepted input power and thereby, the input impedance. Although the dipole input impedance over a lossy half-space has been already derived in closed-form in [16], to author's best knowledge, there exists no such result for the aperture over a lossy half-space. Consequently, one contribution of this paper is to provide an easy-to-compute expression to calculate the aperture's input impedance based on the complex image technique.

Section 2 emphasizes the issue of defining a gain for an antenna that is embedded on the human body. Section 3 defines the alternative properties that will be used in this paper to characterize antenna performance. Section 4 derives the expression of the aperture's input impedance over the human body that is necessary to calculate results presented in Section 5, in terms of link budget and radiation efficiency.

2. GAIN OF A DIPOLE ANTENNA OVER A HUMAN BODY

In this section, we aim to establish the expression of the gain of a vertical dipole placed at a height h_{Tc} above the body skin phantom as illustrated in Figure 1. At 60 GHz, the body can be approximated by a planar homogeneous dissipative medium characterized with body skin dielectric properties from [17]. The two media, air and body phantom, are characterized by their wave numbers k_0 and k_{skin}, respectively. From Figure 1, the direct and reflected path lengths are represented by r_1 and r_2, and can be written as:

$$r_1 = \sqrt{\rho^2 + (h_R - h_{Tc})^2}, \quad r_2 = \sqrt{\rho^2 + (h_R + h_{Tc})^2} \tag{1}$$

In Equation (1), ρ is the horizontal distance, h_R the observation point height above the phantom, and h_{Tc} the separating distance from the phantom surface to the dipole center along its length.

In far-field condition, the distances r_1 and r_2 can be approximate

• for amplitude variations with

$$r_1 \approx r_2 \approx r \tag{2}$$

• and for phase variation with

$$r_1 \approx r - h_{Tc} \cos\theta, \quad r_2 \approx r + h_{Tc} \cos\theta \tag{3}$$

The antenna gain is obtained from the radiated power toward a given direction with respect to the isotropically radiated input power according to equation [18]

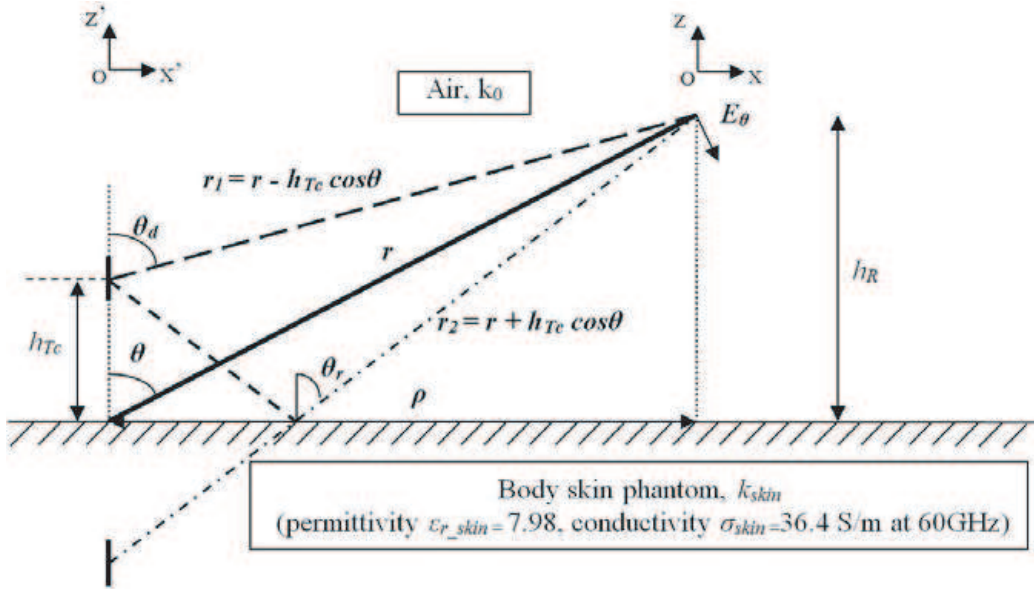$$G_\theta = \frac{4\pi(r|E_\theta|)^2}{2\eta_0 P_{in}} \tag{4}$$

Figure 1. Vertical electric dipole in air at height h_{Tc} over a planar body skin phantom.

where η_0 is the free-space intrinsic impedance, r the radial distance (see Figure 1), P_{in} is the accepted input power, and E_θ the electric far field θ-component. This formulation slightly differs from classical free-space gain definition since the axis reference in Figure 1 is deported from antenna central phase. This approach however has the benefit to be compatible with the definition of the geometry as described in Figure 1, which has been used to derive field expressions over a lossy half-space in an analytical form. For instance, Norton formulation has been shown to correctly define the radiated field for on-body propagation in [19] and is therefore used here to calculate the field E_θ using:

$$E_\theta = E_\rho \cos\theta - E_z \sin\theta \tag{5}$$

where E_ρ and E_z are the cylindrical field components received at an observation point located at a horizontal distance ρ and height h_R from a vertical dipole fed by a constant current I_0 and of length $2l$.

The cylindrical field components are given in [20]. In far-field regio[†], we obtain the total field expression (6), where the commonly negligible first higher-order contribution is retained in the formula in addition to the far-field component $1/r$. Although this second term vanishes in the far field away from the human body, it is not negligible near the air-skin interface, where the $1/r$ far-field term vanishes. The first term is not dependent on the dielectric characteristics and corresponds to the sum of the field radiated in free space and the field reflected by a Perfect Electric Conductor (PEC) located at the air-skin interface. The last term includes the medium effect on wave reflection and the so-called Norton surface wave contributions.

$$E_\theta \approx -\frac{\eta_0}{4\pi}\left(I_0 l\right)\left[\frac{j2k_0 e^{jk_0 r}}{r}\sin\theta\cos\left(k_0 h\cos\theta\right) + 2k_0^2 \upsilon\left(\upsilon\cos\theta - \sin^2\theta\right)e^{jk_0 r_2}\sqrt{\frac{\pi}{k_0 r}}e^{-jP}f_P\right] \tag{6}$$

where υ is the wave number ratio given by (7):

$$\upsilon = \frac{k_0}{k_{skin}} \tag{7}$$

The f_P expression contains the Fresnel integral bounded with numerical distance P:

$$f_P = \frac{1}{2}\left(1+j\right) - \int_0^P \frac{e^{jt}}{\sqrt{2\pi t}}dt \tag{8}$$

$$P = \left(\frac{k_0 r_2}{2}\right)\left(\frac{\upsilon r_2 + z' + z}{\rho}\right)^2 \in \mathbb{C} \tag{9}$$

[†] According to [20], the far-field is defined for $4 < |P| < 8$ and is equivalent to a distance higher than $0.086\,\text{m}$ ($8.6\,\text{cm}$) for on body propagation at $60\,\text{GHz}$.

Applying Eq. (6) into Eq. (4), the final expression of the dipole gain on a lossy dielectric is given by:

$$G_\theta = \frac{\eta_0 (I_0 l)^2}{8\pi P_{in}} \left| j2k_0 e^{jk_0 r} \sin\theta \cos(k_0 h \cos\theta) + 2r k_0^2 \nu \left(\nu \cos\theta - \sin^2\theta\right) e^{jk_0 r_2} \sqrt{\frac{\pi}{k_0 r}} e^{-jP} f_P \right|^2 \quad (10)$$

We notice that when neglecting the second term in Eq. (10), arising from the higher-order term in Eq. (9), the resulting gain expression is the same as the dipole gain above a PEC plane according to the image theory [18]. Unlike these commonly known antenna gains in free space or above a PEC, the gain in Equation (10) depends on the observation distance present in the second term. Consequently, this distance-dependent gain appears not suitable for describing antenna radiation behavior over lossy half-space, especially for the design of on-body links. So, this raises the issue of how to compare the performance of two different antennas once they are embedded on a human body.

To give better insights regarding this issue, two canonical antennas are considered in following sections, namely, one dipole antenna and one aperture antenna. In free space, knowing their gain would be sufficient to design a wireless link accordingly. However, because the human body is a lossy medium, its interaction with the antenna will influence the overall radiation efficiency. So, we propose to calculate the radiated field and observe the link budget and radiation efficiency in order to compare the two canonical antennas, as explained in Section 3.

3. POWER CONSIDERATIONS: LINK BUDGET AND RADIATION EFFICIENCY

The on-body link configuration is presented in Figure 2 for a rectangular aperture or a dipole radiating to a distant point above a body-skin half-space. The considered aperture and dipole have the same dimension along the vertical axis (Oz') and are assumed to be vertically polarized.
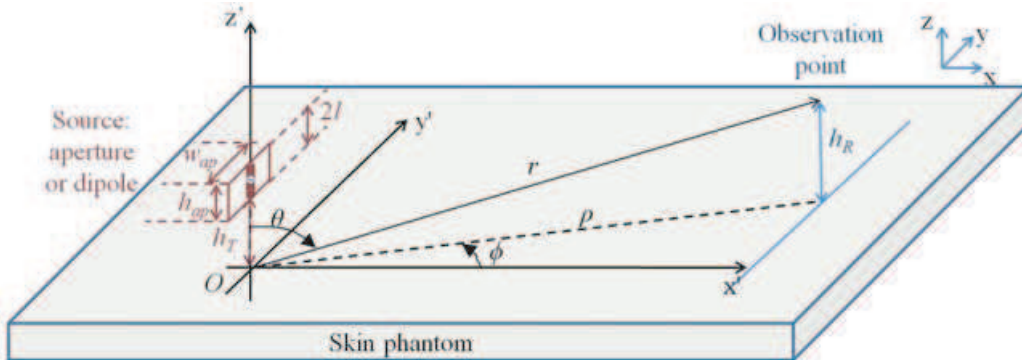

Figure 2. Geometry under investigation: source radiating above the phantom plan $(Ox'y')$.

The body is modeled by a planar half-space corresponding to $(Ox'y')$ plane. The suitability of the planar geometry for on-body links has been validated to some extent using full-wave simulations considering a real human shape up to 60 GHz in [19] and also with measurements from the literature in [21].

At 60 GHz, the skin depth (0.5 mm) is most of the time lower than the skin thickness which may range between 0.5 mm and 1.7 mm, and in most human part equals 1 mm [22, 23]. Therefore, the propagation media can be considered as an infinite half-space.

The received power P_{RX} at the distant observation point depends on the antenna height h_T, source-observation distance ρ, and observation point height h_R. The antenna source height h_T considered here differs from the previous one (h_{Tc} in Figure 1) since it is taken from the phantom surface to the bottom part of the antenna rather than its vertical center.

The basic link budget between two antennas is given by:

$$P_{RX}(\text{dBm}) = P_{TX}(\text{dBm}) - PL(\text{dB}) + G_{TX}(\text{dBi}) + G_{RX}(\text{dBi}) \quad (11)$$

where P_{TX} is the antenna accepted input power, PL the path loss, and the transmitter antenna gain G_{TX} variability was discussed in the previous section. In our case, an observation point is considered at the reception, which is equivalent to an isotropic receiving antenna ($G_{RX} = 0\,\text{dBi}$). The effective area of such an antenna is equal to $\lambda^2/4\pi$. Therefore, the received power can be determined from the radiated field by:

$$P_{RX} = \frac{|E_{RX}|^2}{2\eta_0} \frac{\lambda^2}{4\pi} \tag{12}$$

where η_0 is the intrinsic impedance of free space, and E_{RX} is the radiated field at the receiver location. We define the radiation efficiency as the ratio between P_{rad}, the total radiated power in the upper half space (since the power radiated in the lower half-space is considered not to contribute to the BAN communications, and vanishes anyway in far-field because of the losses), and P_{in}, the antenna real input power:

$$\eta = \frac{P_{rad}}{P_{in}} \tag{13}$$

$$P_{rad} = \frac{1}{2\eta_0} \int_0^{\frac{\pi}{2}} \int_{-\frac{\pi}{2}}^{\frac{\pi}{2}} |E_{RX}|^2 \, r^2 \sin\theta d\theta d\phi \tag{14}$$

with θ, the elevation angle varying in the interval $[-\frac{\pi}{2}, \frac{\pi}{2}]$, φ the azimuthal angle in interval $[0, \frac{\pi}{2}]$, and r the radial distance (cf. Figure 2).

We intend to compare the performances of both the canonical antennas under consideration using the received power P_{RX} given by Equation (12) and the radiation efficiency given in Equation (13). To obtain a meaningful comparison on P_{RX}, both antennas should accept the same amount of power. To ensure that and also to calculate η in Equation (13), the antennas' input impedance Z_{in} over the human body needs to be known. In fact, the power calculation in Equations (12) and (14) is based on the field E_{RX} which itself depends on the current distribution from the relation [16, 24]:

$$E_{RX}(\mathbf{r}) = \frac{1}{j\omega\varepsilon_0} \iint_{S'} \left(k_0^2 + \frac{\partial^2}{\partial z^2} \right) G_A^{zz} J(\mathbf{r}')\mathbf{dS}' \tag{15}$$

- $\mathbf{r}$: observation point vector position;
- $\mathbf{r}'$: source vector position;
- G_A^{zz} : vector Green's function for vector potential due to an infinitesimal dipole orientated along the vertical direction z.
- $J(\mathbf{r}')$: the source current density polarized along z-axis.

For the dipole antenna, neglecting the current variation along φ, the current density J flowing on the cylindrical surface is equivalent to a linear current I distributed along its length as:

$$I(z') = I_0 \sin\left(k_0 \left[l - |z' - (l + h_T)|\right]\right) \tag{16}$$

where l is the dipole half length, z' the source current position, and h_T the dipole height as shown in Figure 2. The constant current I_0 in (16) is related to the accepted input power P_{in} by:

$$I_0 = \sqrt{\frac{2P_{in}}{\text{Re}(Z_{in})}} \tag{17}$$

where Z_{in} is the input impedance.

For an aperture with a TE_{10} mode field distribution, the current density $\mathbf{J}$ is given as follows:

$$\mathbf{J} = J_0 \cos\left(\frac{\pi}{w_{ap}}y'\right) \hat{\mathbf{z}'}, \ y' \in \left[-\frac{w_{ap}}{2}, \frac{w_{ap}}{2}\right] \tag{18}$$

The constant current J_0 is determined from the equivalence principle relating the field in the aperture to the current (factor 2 in Eq. (19)) and the normalizing constant from [25]:

$$J_0 = \left(2\sqrt{\frac{2}{h_{ap}w_{ap}}}\right) \sqrt{\frac{2P_{in}}{\text{Re}(Z_{in})}} \tag{19}$$

where h_{ap} is the dimension along z and w_{ap} the width along y' (cf. Figure 2).

The input impedance of a vertical dipole was determined in [16] using the complex image method. However, to the authors' best knowledge, the input impedance of an aperture over a lossy half-space is not available in the literature. Consequently, we propose to extend the approach of [16] in the next section in order to calculate the input impedance of a vertically polarized aperture over a human body.

4. ANTENNA INPUT IMPEDANCE

The aim of this section is to provide an easy-to-compute formula for the input impedance of a vertically-polarized aperture over a lossy half-space. In [16], the impedance of a vertical dipole on a dielectric is obtained from its current distribution and its radiated E-field by using the EMF (ElectroMotrice Force) method. Assuming a sinusoidal current distribution, the authors of [16] obtained a convenient impedance expression that avoids any singularity problem. This method is also applied here for the rectangular aperture where further singularities due to the double spatial integration have been taken care of.

The aperture input admittance Y_{in} is defined in [18] as:

$$Y_{in} = \frac{2P^*}{|V_{in}|^2} \tag{20}$$

where P is the complex power crossing the aperture, V_{in} the input voltage, and P is obtained by integrating the flux of the Poynting vector through the aperture over the aperture surface:

$$P = \frac{1}{2} \iint (\mathbf{E} \times \mathbf{H}^*) \cdot \hat{\mathbf{n}} \mathbf{ds} \tag{21}$$

In Eq. (21), $\mathbf{H}^*$ is the conjugate of the magnetic field, and $\hat{\mathbf{n}}$ is the normal to the surface vector. The electric field $\mathbf{E}$ is related to the magnetic current distribution M on the aperture according to equivalence principle for an aperture with an infinite PEC around [18] as:

$$\mathbf{M} = -2\hat{\mathbf{n}} \times \mathbf{E} \tag{22}$$

The resulting admittance is therefore:

$$Y_{in} = -\frac{1}{2|V_{in}|^2} \iint_S H(\mathbf{r}) M^*(\mathbf{r}) \mathbf{dS} \tag{23}$$

where $\mathbf{r}$ denotes the vector position at the observation point.

The radiated magnetic field from a rectangular surface is defined by Pocklington's integral [24] as:

$$H(\mathbf{r}) = \frac{1}{j\omega\mu_0} \iint_{S'} \left[k_0^2 \overline{\overline{G_A}}(\mathbf{r}|\mathbf{r}') - \nabla\nabla' G_q(\mathbf{r}|\mathbf{r}') \right] \mathbf{M}(\mathbf{r}') \mathbf{dS}' \tag{24}$$

- $\overline{\overline{G_A}}$: dyadic Green function for vector potential;
- Gq: Green function for scalar potential.

The other parameters are the same as in Eq. (15). For a horizontally oriented magnetic infinitesimal dipole (i.e., vertical polarization of the electric field):

$$\overline{\overline{G_A}}(\mathbf{r}|\mathbf{r}') = \hat{y}\hat{y} G_A^{yy} \tag{25}$$

$$H(\mathbf{r}) = \underbrace{\frac{1}{j\omega\mu_0} \iint_{S'} k_0^2 G_A^{yy} \mathbf{M}(\mathbf{r}') \mathbf{dS}'}_{H_A} - \underbrace{\frac{1}{j\omega\mu_0} \iint_{S'} \nabla\nabla' G_q(\mathbf{r}|\mathbf{r}') \mathbf{M}(\mathbf{r}') \mathbf{dS}'}_{H_V} \tag{26}$$

Subscripts A and V denote terms related to vector and scalar potentials, respectively, and the input admittance can then also be separated into vector and scalar terms such as:

$$Y_{in} = Y_{in}^A + Y_{in}^V, \tag{27}$$

$$Y_{in}^A = -\frac{1}{2|V_{in}|^2} \iint_S H_A(\mathbf{r}) \mathbf{M}^*(\mathbf{r}) \mathbf{dS} \tag{28}$$

$$Y_{in}^V = -\frac{1}{2|V_{in}|^2} \iint_S H_V(\mathbf{r}) \mathbf{M}^*(\mathbf{r}) \mathbf{dS} \tag{29}$$

For a TE_{10} propagation mode, the magnetic current distribution M is defined by Eq. (30):

$$\mathbf{M} = M_0 \cos\left(\frac{\pi}{w_{ap}} y'\right) \hat{\mathbf{y}}', \ y' \in \left[-\frac{w_{ap}}{2}, \frac{w_{ap}}{2}\right] \tag{30}$$

The maximum current M_0 is related to the input voltage using the same approach than for the constant current J_0 in Eq. (19):

$$\frac{M_0}{V_{in}} = 2\sqrt{\frac{2}{w_{ap} h_{ap}}} \tag{31}$$

After combining Eqs. (30)–(31) with Eqs. (28)–(29), the obtained input-admittance vector and scalar terms are respectively:

$$Y_{in}^A = -\frac{4k_0^2}{j\omega\mu_0 w_{ap} h_{ap}} \int_{h_R}^{h_R+h_{ap}} dz \int_{h_T}^{h_T+h_{ap}} dz' \int_{-w_{ap}/2}^{w_{ap}/2} dy \int_{-w_{ap}/2}^{w_{ap}/2} dy' \left[\cos\left(\frac{\pi}{w_{ap}} y\right) G_A^{yy} \cos\left(\frac{\pi}{w_{ap}} y'\right)\right] \tag{32}$$

$$Y_{in}^V = \frac{4}{j\omega\mu_0 w_{ap} h_{ap}} \int_{h_R}^{h_R+h_{ap}} dz \int_{h_T}^{h_T+h_{ap}} dz' \int_{-w_{ap}/2}^{w_{ap}/2} dy \int_{-w_{ap}/2}^{w_{ap}/2} dy' \left[\cos\left(\frac{\pi}{w_{ap}} y\right) \nabla\nabla' G_q \cos\left(\frac{\pi}{w_{ap}} y'\right)\right] \tag{33}$$

The double operator $\nabla\nabla'$ applied on G_q can be simplified in Eq. (33) by integrating by parts (cf. Appendix A):

$$Y_{in}^V = \frac{4\left(\frac{\pi}{w_{ap}}\right)^2}{j\omega\mu_0 w_{ap} h_{ap}} \int_{h_R}^{h_R+h_{ap}} dz \int_{h_T}^{h_T+h_{ap}} dz' \int_{-w_{ap}/2}^{w_{ap}/2} dy \int_{-w_{ap}/2}^{w_{ap}/2} dy' \left[\sin\left(\frac{\pi}{w_{ap}} y\right) G_q \sin\left(\frac{\pi}{w_{ap}} y'\right)\right] \tag{34}$$

The Green's functions G_A^{yy} and G_q expressions are obtained considering the duality between electric and magnetic field using expressions given in [26]:

$$G_A^{yy} = \frac{1}{4\pi} \int_{-\infty}^{\infty} \frac{1}{j2k_{z0}} \left(e^{-jk_{z0}(z-z')} - Ke^{-jk_{z0}(z+z')} + \tilde{f}_1(k_{z0}) e^{-jk_{z0}(z+z')}\right) H_0^{(2)}(k_\rho\rho) k_\rho dk_\rho \tag{35}$$

$$G_q = \frac{1}{4\pi} \int_{-\infty}^{\infty} \frac{1}{j2k_{z0}} \left(e^{-jk_{z0}(z-z')} + \tilde{f}_2(k_{z0}) e^{-jk_{z0}(z+z')}\right) H_0^{(2)}(k_\rho\rho) k_\rho dk_\rho \tag{36}$$

where k_ρ is the radial-component wavenumber, $H_0^{(2)}$ the Hankel function of second kind and zeroth order, ρ the radial distance $\rho = \sqrt{(x-x')^2 + (y-y')^2}$, and K the reflection coefficient:

$$K = \frac{1 - \varepsilon_{rc}}{1 + \varepsilon_{rc}} \tag{37}$$

In Eq. (37), ε_{rc} represents the dielectric complex permittivity defined as:

$$\varepsilon_{rc} = \varepsilon_{r\_skin} - j\frac{\sigma_{skin}}{\omega} \tag{38}$$

The spectral functions $\tilde{f}_i$ are given by the following expressions:

$$\tilde{f}_1(k_{z0}) = -\frac{k_{z\_skin} - \varepsilon_{rc}k_{z0}}{k_{z\_skin} + \varepsilon_{rc}k_{z0}} + K \tag{39}$$

$$\tilde{f}_2(k_{z0}) = (\varepsilon_{rc} - 1)\frac{k_{z0}(k_{z\_skin} - k_{z0})}{(k_{z\_skin} + k_{z0})(k_{z\_skin} + \varepsilon_{rc}k_{z0})} + \frac{(k_{z0} - k_{z\_skin})}{(k_{z\_skin} + \varepsilon_{rc}k_{z0})} \tag{40}$$

In these equations k_{z0} and k_{z_skin} are the z-directed wavenumbers defined as follow:

$$k_{z0}^2 + k_\rho^2 = k_0^2, \quad k_{z\_skin}^2 + k_\rho^2 = \varepsilon_{rc}k_0^2. \tag{41}$$

It is well known that the Sommerfeld integrals in Eqs. (35) and (36) are slowly convergent and will be consequently evaluated using the complex image technique [16, 27]. Each spectral function

$\tilde{f}_i(k_{z0})$, $(i = 1, 2)$ is approximated by a short series of exponential functions with complex coefficients a_{ij}, b_{ij}:

$$\tilde{f}_{i(i=1,2)}(k_{z0}) = a_{i1}e^{b_{i1}k_{z0}} + a_{i2}e^{b_{i2}k_{z0}} + \ldots + a_{iN}e^{b_{iN_i}k_{z0}} \tag{42}$$

The complex coefficients are obtained from Matrix Pencil method [28]. The number N_i of terms in the series is chosen in such a way to minimize the approximation error (between Eqs. (39)–(40) and (42) and is usually found to be about $12 \sim 13$ for the scenario investigated in this paper).

By substituting the spectral functions in Eqs. (35)–(36) with Eq. (42) and applying the Sommerfeld identity [29, 30], we obtain:

$$G_A^{yy} = \underbrace{\frac{e^{-jk_0R_s}}{4\pi R_s}}_{source\ term} - \underbrace{K\frac{e^{-jk_0R_q}}{4\pi R_q}}_{quasi\text{-}static\ term} + \underbrace{\sum_{j=1}^{N_1}a_{1j}\frac{e^{-jk_0R_{1j}}}{4\pi R_{1j}}}_{complex\ images\ term}, \quad N_1 = 12 \sim 13 \tag{43}$$

$$G_q = \underbrace{\frac{e^{-jk_0R_s}}{4\pi R_s}}_{source\ term} + \underbrace{\sum_{j=1}^{N_2}a_{2j}\frac{e^{-jk_0R_{2j}}}{4\pi R_{2j}}}_{complex\ images\ term}, \quad N_2 = 12 \sim 13 \tag{44}$$

$$\text{with} \quad R_s = \left[\Delta x^2 + (y-y')^2 + (z-z')^2\right]^{1/2} \tag{45}$$

$$R_q = \left[\Delta x^2 + (y-y')^2 + (z+z')^2\right]^{1/2} \tag{46}$$

$$R_{ij} = \left[\Delta x^2 + (y-y')^2 + (z+z'-jb_{ij})^2\right]^{1/2} \tag{47}$$

The Green's functions are composed of a source term representing the direct wave, a quasi-static term representing the reflected wave (only for G_A^{yy}), and a series of complex image terms. This latter term accounts for the diffraction that occurs at the skin/air interface due to the fast-varying behavior of the reflection coefficient at grazing angles in the Sommerfeld integral [31]. Such a formulation can be illustrated as in Figure 3.

Figure 3. Complex image components for an aperture antenna.

In Figure 3, the aperture radiating above a lossy half-space is equivalent to an array composed of the original source, the quasi-static image, and a series of complex images, all source and images radiating in homogenous free space.

The input admittance is computed for observation points forming an aperture in front of the radiating aperture and spaced with an infinitesimal distance Δx from the source. Therefore, a singularity is encountered when trying to solve the quadruple integration in Eqs. (32)–(34) using Green's functions in Eqs. (43)–(44) for R_S tends to 0 (meaning that the elementary source and the observation point are almost at the same position). To avoid this singularity, a change of variable $\sigma = y - y'$ is performed and leads to the following expressions of the vector term (from Eq. (32)):

$$Y_{in}^A = -\frac{4k_0^2}{j\omega\mu_0 w_{ap}h_{ap}} \int_{h_R}^{h_R+h_{ap}} \int_{h_T}^{h_T+h_{ap}} \left\{ \int_{-w_{ap}}^{0} G_A^{yy}\varphi_1(\sigma)\,d\sigma + \int_{0}^{w_{ap}} G_A^{yy}\varphi_2(\sigma)\,d\sigma \right\} dz'dz \qquad (48)$$

where

$$\varphi_1(\sigma) = \cos\left(\frac{\pi\sigma}{w_{ap}}\right)\left(\frac{w_{ap}}{\pi}\right)\left[\frac{\pi}{2a}(\sigma+w_{ap}) - \frac{1}{4}\sin\left(\frac{2\pi\sigma}{w_{ap}}\right)\right] - \sin\left(\frac{\pi\sigma}{w_{ap}}\right)\left(\frac{w_{ap}}{4\pi}\right)\left[1 - \cos\left(\frac{2\pi\sigma}{w_{ap}}\right)\right], \qquad (49)$$

$$\varphi_2(\sigma) = \cos\left(\frac{\pi\sigma}{w_{ap}}\right)\left(\frac{w_{ap}}{\pi}\right)\left[\frac{\pi}{2w_{ap}}(-\sigma+w_{ap}) + \frac{1}{4}\sin\left(\frac{2\pi\sigma}{w_{ap}}\right)\right] + \sin\left(\frac{\pi\sigma}{w_{ap}}\right)\left(\frac{w_{ap}}{4\pi}\right)\left[1 - \cos\left(\frac{2\pi\sigma}{w_{ap}}\right)\right], \qquad (50)$$

and the scalar term (from Eq. (34)):

$$Y_{in}^V = \frac{4\left(\frac{\pi}{w_{ap}}\right)^2}{j\omega\mu_0 w_{ap}h_{ap}} \int_{h_R}^{h_R+h_{ap}} \int_{h_T}^{h_T+h_{ap}} \left\{ \int_{-w_{ap}}^{0} G_q\psi_1(\sigma)\,d\sigma + \int_{0}^{w_{ap}} G_q\psi_2(\sigma)\,d\sigma \right\} dz'dz \qquad (51)$$

where

$$\psi_1(\sigma) = \cos\left(\frac{\pi\sigma}{w_{ap}}\right)\left(\frac{w_{ap}}{\pi}\right)\left[\frac{\pi}{2w_{ap}}(\sigma+w_{ap}) + \frac{1}{4}\sin\left(\frac{2\pi\sigma}{w_{ap}}\right)\right] + \sin\left(\frac{\pi\sigma}{w_{ap}}\right)\left(\frac{w_{ap}}{4\pi}\right)\left[1 - \cos\left(\frac{2\pi\sigma}{w_{ap}}\right)\right], \qquad (52)$$

$$\psi_2(\sigma) = \cos\left(\frac{\pi\sigma}{w_{ap}}\right)\left(\frac{w_{ap}}{\pi}\right)\left[\frac{\pi}{2w_{ap}}(-\sigma+w_{ap}) - \frac{1}{4}\sin\left(\frac{2\pi\sigma}{w_{ap}}\right)\right] - \sin\left(\frac{\pi\sigma}{w_{ap}}\right)\left(\frac{w_{ap}}{4\pi}\right)\left[1 - \cos\left(\frac{2\pi\sigma}{w_{ap}}\right)\right]. \qquad (53)$$

The final expression of the total input impedance is consequently:

$$Y_{in} = \frac{4\,(j\omega\varepsilon_0)}{w_{ap}h_{ap}} \int_{h_R}^{h_R+h_{ap}} \int_{h_T}^{h_T+h_{ap}} \left\{ \int_{-w_{ap}}^{0} G_A^{yy}\varphi_1(\sigma)\,d\sigma + \int_{0}^{w_{ap}} G_A^{yy}\varphi_2(\sigma)\,d\sigma \right\} dz'dz$$

$$+ \frac{4\left(\frac{\pi}{w_{ap}}\right)^2}{j\omega\mu_0 w_{ap}h_{ap}} \int_{h_R}^{h_R+h_{ap}} \int_{h_T}^{h_T+h_{ap}} \left\{ \int_{-w_{ap}}^{0} G_A^{yy}\psi_1(\sigma)\,d\sigma + \int_{0}^{w_{ap}} G_A^{yy}\psi_2(\sigma)\,d\sigma \right\} dz'dz \qquad (54)$$

The integral in Eq. (54) is convergent since we reduce the singularity order from 4 to 3. When evaluating the inner zz' integral in Eq. (54) with different values of $\Delta x < \lambda/10^6$ (very close to the actual aperture plane) for Eqs. (45)–(47), a constant admittance is obtained, which confirms that convergence is achieved. One can assume that the calculated admittance is the input admittance of the aperture considering the extremely low value of $\Delta x\,(< \lambda/10^6)$.

The input impedance of a standard WR15 ($3.76 \times 1.88\,\text{mm}^2$ size) waveguide aperture with a TE_{10} field distribution operating at $60\,\text{GHz}$ is computed by inversing the admittance from Equation (54) for different heights h_T ranging from 0 to $10\,\text{mm}$ above the body skin. For validation, the result is compared with the impedance of the same aperture obtained from CST Microwave Studio with time domain solver. The simulated structure is shown in Figure 4. A WR15 waveguide is placed above the middle of a phantom. Since the theoretical calculation of the impedance assumes an infinite PEC around the aperture (like with classical apertures radiating in free space [18]), we simulated the aperture also with a PEC around (touching the boundary box) in order to validate Equation (54) with a geometry as close as possible to the one theoretically assumed. The phantom size is fixed at $200 \times 200 \times 3\,\text{mm}^3$ (no changes are observed on the input impedance when the phantom exceeds this size). The impedance of
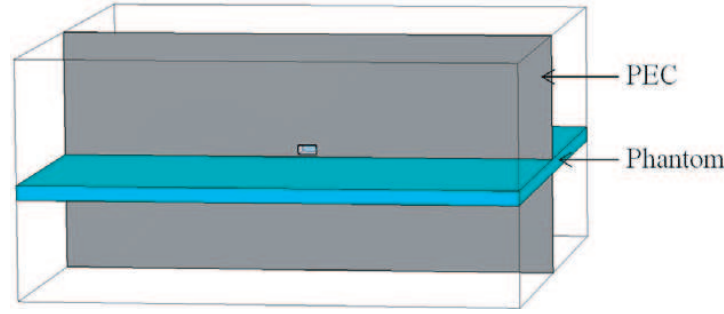
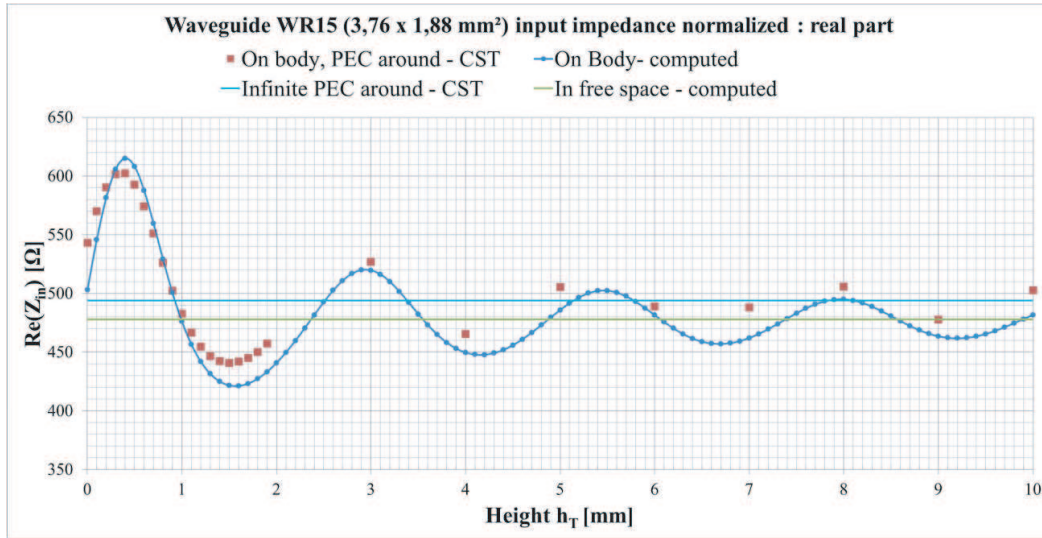**Figure 4.** Simulated aperture structure in CST Microwave Studio.

Figure 5. Computed and simulated input impedance real part variation along the height h_T at 60 GHz.

an aperture with an infinite PEC around radiating in free space is also computed using the theoretical formulation in [25] and simulated with CST Microwave Studio to show that at higher height on body skin phantom, the obtained impedance tends to the one in free space. The resulting input impedance variation with respect to the aperture height above the body skin phantom is shown in Figure 5 and Figure 6. The aperture input impedance exhibits a sinusoidal variation along antenna heights above the body with a half-wavelength period around the free-space input impedance. The amplitude decreases with the antenna height and tends to the free space aperture impedance. The difference between computed result and CST results is always less than 5% for both real and imaginary parts.

In the scenario considered in this paper, i.e., operation frequency at 60 GHz, a single layer of skin is sufficient to model on-body propagation. However, for lower frequencies, multi-layer geometry including other human tissues (e.g., fat, muscle) has to be considered. To solve the integral in Equation (54), we provide additional material in Appendix B to consider triple-layer geometry (i.e., skin/fat/muscle).

5. LINK BUDGET AND EFFICIENCY RESULTS

5.1. Radiated Power

Knowing the input impedance (its real part in particular) and assuming no loss resistance, it is now possible to calculate the field radiated by the dipole and the aperture antenna, with both accepting the same input power P_{in}, using Equations (17) and (19). Firstly, the path loss between antennas
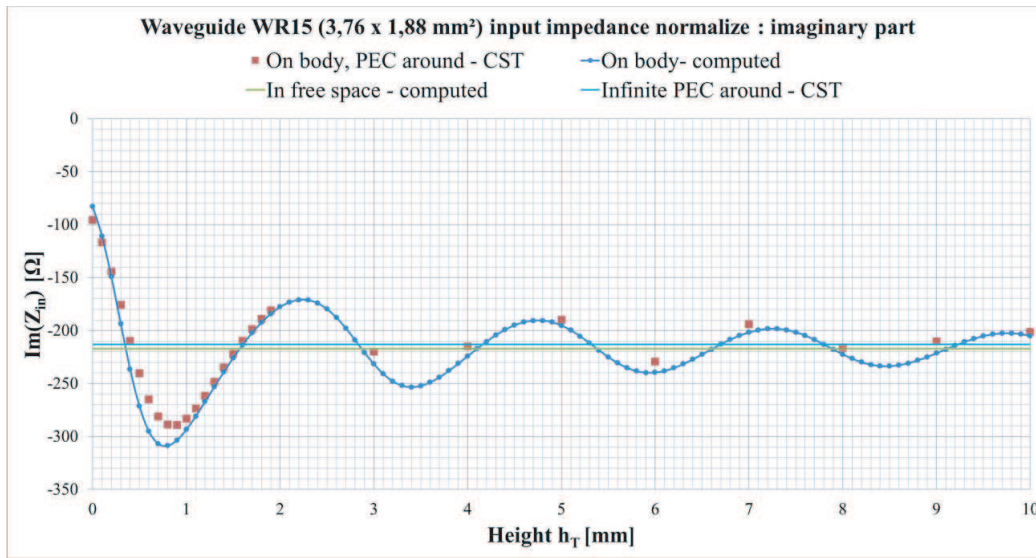
Figure 6. Computed and simulated input impedance imaginary part variation along the height h_T at 60 GHz.
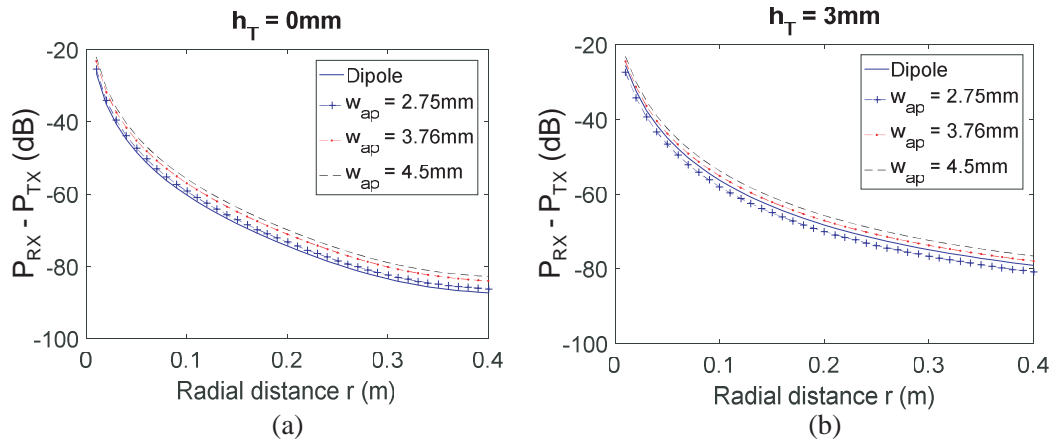

Figure 7. Path loss between antennas and observation point on body skin dielectric phantom $(h_R = 0\,\text{mm})$ for different transmitter height: (a) $h_T = 0\,\text{mm}$, (b) $h_T = 3\,\text{mm}$.

and an observation point located on the skin/air interface (i.e., $h_R = 0\,\text{mm}$) is plotted for antenna height $h_T = 0\,\text{mm}$ and $h_T = 3\,\text{mm}$ in Figures 7(a) and 7(b) respectively. Results for the dipole and for three different aperture widths are given. Aperture widths are limited by TE_{10} monomode propagation constraint.

When $h_T = 0\,\text{mm}$, the path loss is greater with the dipole, and the received power is the largest with the widest aperture. The difference between the received powers from a dipole and an aperture at different observation positions increases with the aperture width from $1\,\text{dB}$ ($w_{ap} = 2.75\,\text{mm}$) to $4.5\,\text{dB}$ ($w_{ap} = 4.5\,\text{mm}$). When $h_T = 3\,\text{mm}$, while the widest aperture exhibits the best performance, it is to be noted that the dipole performs better than the 2.75-mm-wide aperture (by about $1.8\,\text{dB}$ at $r = 40\,\text{cm}$). The attenuation at $r = 40\,\text{cm}$ is higher ($87.3\,\text{dB}$) for antennas in direct contact to the body skin phantom than at $h_T = 3\,\text{mm}$ ($80.8\,\text{dB}$).

The angular variation of the path loss is now investigated. The azimuthal variation along the skin/air interface is shown in Figure 8 and the elevation pattern shown in Figure 9.

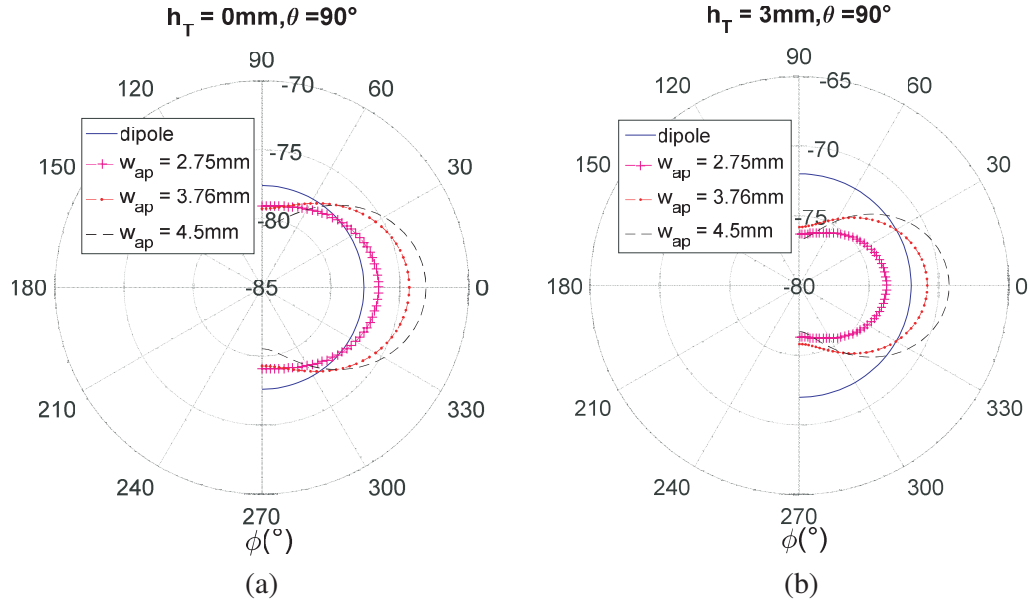In the azimuth plane, the field is plotted only in the forward space. The dipole exhibits an

Figure 8. Path loss in the azimuth plane for a radial distance $r = 25\,\mathrm{m}$: (a) $h_T = 0\,\mathrm{mm}$, (b) $h_T = 3\,\mathrm{mm}$ (see coordinate system in Figure 2).
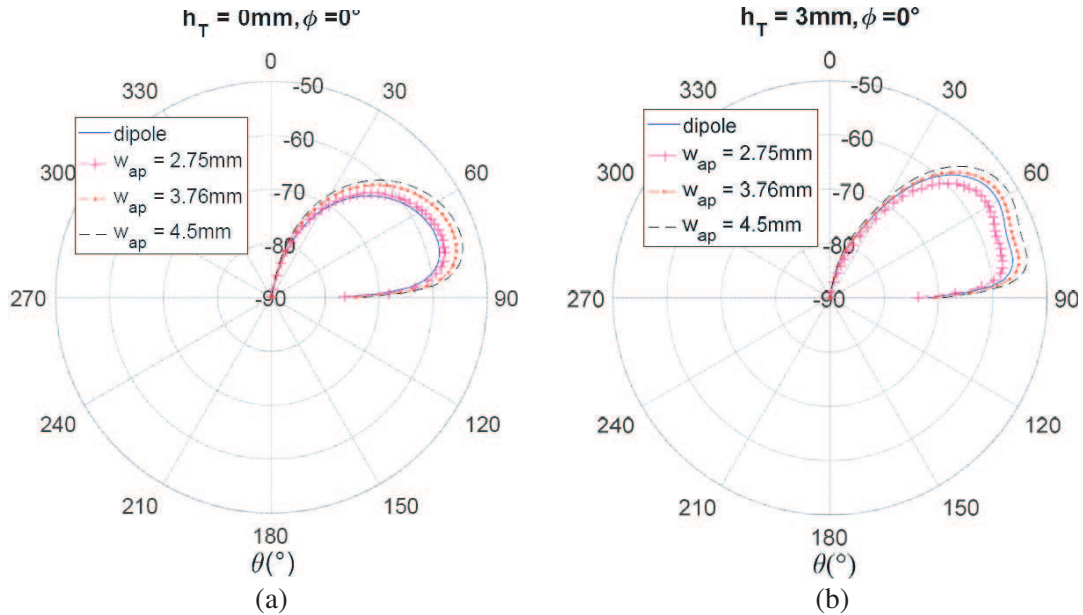
Figure 9. Received power in the elevation plane for radial distance $r = 25\,\mathrm{cm}$: (a) $h_T = 0\,\mathrm{mm}$, (b) $h_T = 3\,\mathrm{mm}$ (see coordinate system in Figure 2).

omnidirectionally radiated field and the apertures have their maximum radiation at ϕ equals to $0°$ for all cases. It is interesting to note that the 2.75 mm-width aperture placed at $h_T = 3\,\mathrm{mm}$ radiates less power than the dipole at $\theta = 90°$ and $r = 25\,\mathrm{cm}$. The aperture $-3\,\mathrm{dB}$ beamwidths are presented in Table 1.

As in free space, the beamwidth decreases with the aperture width. It is to be noted that when $w_{ap} = 2.75\,\mathrm{mm}$, the directivity is so low that a variation of less than $3\,\mathrm{dB}$ is observed over the whole azimuthal angular range. This is why the $-3\,\mathrm{dB}$ beamwidth is equal to $180°$. In the elevation plan

Table 1. $-3\,\mathrm{dB}$ beamwidth in the azimuth plane.

Aperture width	$\mathbf{h_T = 0\,mm}$	$\mathbf{h_T = 3\,mm}$
$\mathbf{w_{ap} = 2.75\,mm}$	180°	180°
$\mathbf{w_{ap} = 3.76\,mm}$	96°	104°
$\mathbf{w_{ap} = 4.5\,mm}$	84°	82°

(normal to the dielectric plane), the main lobe is 30° up-tilted for all cases in Figure 9. The beamwidth is a bit larger for $h_T = 3\,\mathrm{mm}$. As observed previously in the azimuth plane, the smallest aperture radiates less power than the vertical dipole at this height (see Figure 9(b)).

In the case of off-body links, i.e., a link between an on-body antenna and a remote base station, a performance characterization in terms of radiation efficiency may constitute a more useful criterion. Indeed, since humans are moving, the orientation of the on-body antenna with respect to the one of the base station will vary with time. So, assessing the antenna radiated power toward one particular direction appears less suitable than assessing the overall radiation efficiency. Consequently, dipole and aperture antennas' efficiencies are computed, and the results are discussed in the next section.

5.2. Radiation Efficiency

The radiation efficiency has been computed for both the vertical dipole [11] and the vertically polarized aperture at different heights h_T above the body in the 60 GHz-band. It is defined in Eq. (13) by the ratio between the radiated and input powers. The radiated power P_{rad} has been obtained with Eq. (14) using the far field in the upper half-space given in Eq. (15) (with a distance r equal to 100 m). In far field, the main contribution in the field is from direct and reflected waves. The constant currents for the current density in the field expression (15) for each antenna are normalized to fix the accepted input power at 1 W, knowing the input impedance thanks to Equations (17)–(19). The radiation efficiencies at different frequencies around 60 GHz and at different heights h_T above the body skin phantom are plotted separately for a vertical dipole antenna and the standard WR15 waveguide in Figure 10. Figure 11 shows the radiation efficiency variation along the height h_T for all considered antennas.The efficiency has also been simulated in CST for the aperture with standard waveguide dimensions WR15 at four different heights h_T above the body phantom, 0 mm, 3 mm, 5 mm and 10 mm. For different phantom sizes ($50 \times 50 \times 3\,\mathrm{mm}^3$ and $100 \times 100 \times 3\,\mathrm{mm}^3$), the same result is obtained proving that farfield conditions are respected. Simulated results are shown in Figure 11 where a good agreement is obtained with the efficiency computed from Equations (13)–(15).

For a given configuration, Figure 10 shows that the radiation efficiency does not vary much over
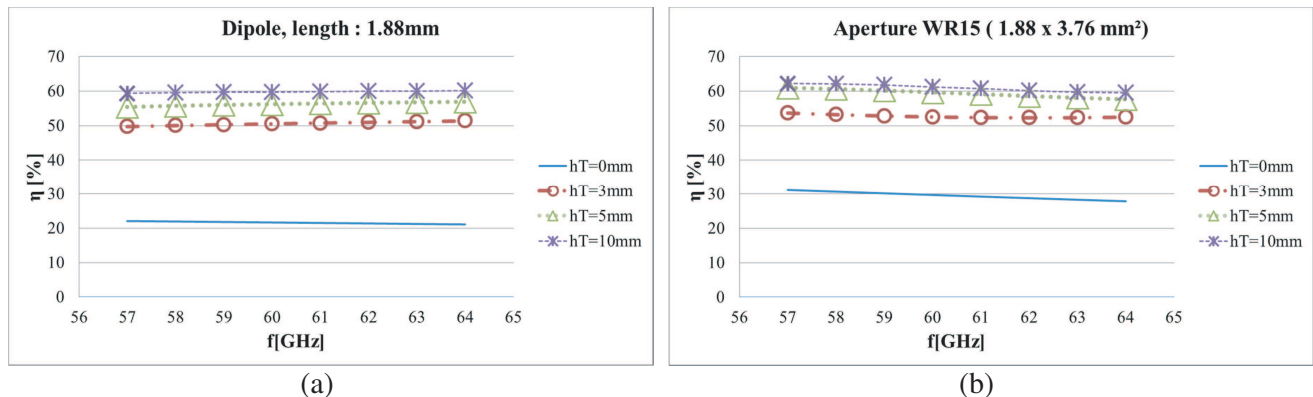

Figure 10. Radiation efficiency in [%] at different height above the body skin phantom: (a) dipole (length $l = 1.88\,\mathrm{mm}$); (b) aperture WR15: $1.88 \times 3.76\,\mathrm{mm}^2$.
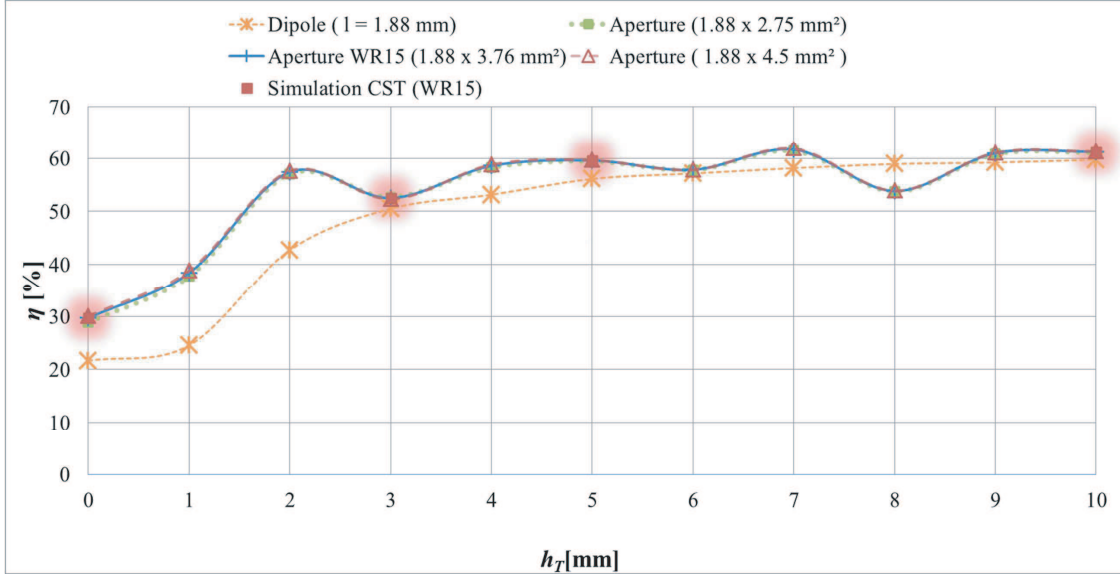
Figure 11. Radiation efficiency in [%] at different height above the body skin phantom at 60 GHz: computed and simulated results.

the 60 GHz license-free bandwidth[‡]. The variation is less than 3.5% in all cases. The efficiency is significantly lower when antennas are located at $h_T = 0$ mm, about 20% (-7 dB) for the dipole and 30% (-5.2 dB) for the apertures, than when located at higher height, reaching about 60% (-2.2 dB) for all antennas in Figure 10 and Figure 11. In general, a large difference is observable by moving the antenna at 3 mm above the skin. The largest aperture is the most efficient when being placed in direct contact to the skin but with a slight difference compared to the two other apertures. Finally, the dipole, as the smallest antenna, presents the lowest efficiency. However, for heights greater than 3 mm above the skin, there are no large differences among antennas, and all efficiencies converge toward 60% (-2.2 dB).

The on-body efficiencies reported for antenna operating around 60 GHz are quite different depending on the antenna type and polarization. Some measurements are in good agreement with our results for a low profile antenna in [32] exhibiting an efficiency of 10% at $h_T = 0$ mm, 30% at $h_T = 1$ mm and 63% at $h_T = 6$ mm. The efficiency variation with respect to the antenna-body spacing is also observed for a SIW (Substrate Integrated Waveguide) multi-directional antenna in [33]. The efficiency decreases from 91% (in free space) to 9% when touching the body, reaches 47% at a height h_T higher than 1 mm, and tends to 60% at $h_T = 5$ mm, which agrees pretty well to the results presented in Figure 11.

5.3. Discussion

When touching the human body, the vertically polarized aperture antenna that exhibits some directivity appears to perform better in terms of radiation efficiency than the quasi-omnidirectional vertically polarized dipole antenna. However, when a spacing distance of about 3 mm (i.e., 0.6λ) is observed, there is no real benefit of the aperture over the dipole. Also, it is interesting to note that a wider aperture that naturally leads to higher directivity does not exhibit higher radiation efficiency and in the frame of BAN, would not be in general useful, considering the fact that the position of the communicating nodes is usually not known due to the moving nature of the human body. So, in the considered scenario, it appears that the radiation efficiency improvement is not related to the directivity but to the current distribution itself.

It is also interesting to note that although the dipole performs slightly better than the $w_{ap} = 2.75$ mm-aperture in Figure 8 and Figure 9 for $h_T = 3$ mm in terms of received power at $r = 0.25$ m, we can see in Figure 11 that the radiation efficiency of the $w_{ap} = 2.75$ mm-aperture is yet slightly higher

---

[‡] The frequency dispersion of the skin's complex permittivity is taken into account using [17].

than the dipole one. So, although the radiation efficiency determined in far-field like in Figure 11 can be a good indicator of performance of on-body antennas for off-body links, it is less appropriate when evaluating the link budget for on-body communications, i.e., when both nodes are placed on the human body. The information of the local diffraction that occurs near the skin/air interface is lost in far field whereas it can contribute to the on-body link.

6. CONCLUSION

The gain dependence on the distance for an elementary dipole radiating on a lossy dielectric was first established. For Body Area Network, this constitutes a limitation to de-embed antenna characteristics from body channel or to compare antenna characteristics once on the body. Consequently, a theoretical approach was conducted to compare a vertical dipole and rectangular aperture antenna radiation on a planar body skin phantom at $60\,\mathrm{GHz}$. To establish the performance in terms of link budget and radiation efficiency, it was necessary to normalize the accepted power for both the antennas. To do so, the aperture input impedance has been derived into a fast-convergent integral that is easy to compute, based on the complex image technique. The aperture has been found to exhibit higher radiation efficiency with respect to the dipole when antennas are located very close to the human body ($< 0.6\lambda$). However, increasing the size of the aperture, and hence its directivity, did not increase the efficiency, which suggests that only the complete current spatial distribution does influence the amount of power that is lost into the human body. When the dipoles and the different apertures were located more than 0.6λ away from the body, no significant differences were found between them and the efficiency was about 60%. Further perspectives of this work aim at investigating the radiation efficiency with horizontally polarized current distributions and other antenna structures.

APPENDIX A. VECTOR TERM SIMPLIFICATION IN THE APERTURE ADMITTANCE

The H-field potential term is given in Eq. (26) by:

$$H_V = -\frac{1}{j\omega\mu_0}\nabla \iint_{S'} \nabla' G_q\left(\mathbf{r}|\mathbf{r}'\right) M\left(\mathbf{r}'\right) dS' \tag{A1}$$

When integrating by parts:

$$H_V = -\frac{1}{j\omega\mu_0}\nabla\left\{\underbrace{\int_{dl} G_q(\mathbf{r}|\mathbf{r}')M(\mathbf{r}')d\hat{n}}_{=0} - \iint_{S'} G_q\left(\mathbf{r}|\mathbf{r}'\right) \nabla' M\left(\mathbf{r}'\right) dS'\right\} \tag{A2}$$

$d\hat{n}$ is the elementary vector normal to the aperture surface, and dl is the aperture contour. $M(\mathbf{r}')$ has a non-zero component along y-axis, but its component is null on the contour since $M(\mathbf{r}') = M_0 \cos\left(\frac{\pi y'}{w_{ap}}\right)\cdot\hat{y}'$.

$$H_V = \frac{1}{j\omega\mu_0}\nabla \iint_{S'} G_q\left(\mathbf{r}|\mathbf{r}'\right) M_0 \left(\frac{\pi}{w_{ap}}\right)\left(-\sin\left(\frac{\pi y'}{w_{ap}}\right)\right) dS' \tag{A3}$$

thus,

$$Y_{in}^V = \frac{1}{j\omega\mu_0 2\left|V_{in}\right|^2} \iint_S \left\{\nabla \iint_{S'} G_q\left(\mathbf{r}|\mathbf{r}'\right) M_0 \left(\frac{\pi}{w_{ap}}\right)\sin\left(\frac{\pi y'}{w_{ap}}\right) dS'\right\} M^*\left(\mathbf{r}\right) dS \tag{A4}$$

By integrating by part a second time:

$$Y_{in}^V = -\frac{1}{j\omega\mu_0 2 |V_{in}|^2} \left\{ \int_{dl} \left[\iint_{S'} G_q\left(\mathbf{r}|\mathbf{r}'\right) M_0\left(\frac{\pi}{w_{ap}}\right)\left(-\sin\left(\frac{\pi y'}{w_{ap}}\right)\right) dS' \right] \underbrace{M_0 \cos\left(\frac{\pi y}{w_{ap}}\right) \hat{y} \cdot d\hat{n}}_{=0} \right.$$

$$\left. - \iint_S \left\{ \iint_{S'} G_q\left(\mathbf{r}|\mathbf{r}'\right) M_0\left(\frac{\pi}{w_{ap}}\right)\left(-\sin\left(\frac{\pi y'}{w_{ap}}\right)\right) dS' \right\} \nabla\left(M_0 \cos\left(\frac{\pi y}{w_{ap}}\right)\right) dS \right\}$$

$$Y_{in}^V = \frac{M_0^2 \left(\frac{\pi}{w_{ap}}\right)^2}{j\omega\mu_0 2 |V_{in}|^2} \iint_S \iint_{S'} G_q\left(\mathbf{r}|\mathbf{r}'\right) \sin\left(\frac{\pi y'}{w_{ap}}\right) \sin\left(\frac{\pi y}{w_{ap}}\right) dS' dS$$

when substituting $\frac{M_0}{V_{in}}$ with Eq. (31), we will obtain (34).

APPENDIX B. IMPEDANCE ON A MULTILAYER

To take into account the body multilayer structure, the complex image functions in Eqs. (39) and (40) are redefined. The Green functions expressions, G_A^{yy} and G_q, remain the same as in Eqs. (43) and (44). K is the amplitude of the quasi-static image defined previously by Eq. (37). The spectral functions $\tilde{f}_i$ include the multilayer structure and become:

$$\tilde{f}_1(k_{z0}) = -\Gamma_{TM} + K \tag{B1}$$

$$\Gamma_{TM} = \frac{Z_{skin\_top} - Z_{0\_air}}{Z_{skin\_top} + Z_{0\_air}} \tag{B2}$$

$$\tilde{f}_2(k_{z0}) = \left(\frac{\varepsilon_{r\_skin} - 1}{\varepsilon_{\_skin}}\right) \frac{Z_{0\_air}\left(Z_{skin\_top}\varepsilon_{r\_skin} - Z_{0\_air}\right)}{\left(Z_{skin\_top}\varepsilon_{r\_skin} + Z_{0\_air}\right)\left(Z_{skin\_top} + Z_{0\_air}\right)}$$
$$- \left(\frac{1}{\varepsilon_{\_skin}}\right) \frac{\left(Z_{skin\_top}\varepsilon_{r\_skin} - Z_{0\_air}\right)}{\left(Z_{skin\_top} + Z_{0\_air}\right)} \tag{B3}$$

where Z_{0_air} is the air impedance, and Z_{skin_top} is the surface impedance at the top of the skin. Iteratively for each layer, the impedances are defined according to the following relations:

$$Z_{0\_layer} = \frac{k_{z\_layer}}{\omega\varepsilon_0\varepsilon_{r\_layer}} \tag{B4}$$

$$Z_{layer\_top} = Z_{0\_layer} \frac{Z_{sub\_layer\_top} + jZ_{0\_layer}\tan\left(k_{z\_layer}h_{layer}\right)}{Z_{0\_layer} + jZ_{sub\_layer\_top}\tan\left(k_{z\_layer}h_{layer}\right)} \tag{B5}$$

$$k_{z\_layer} = \sqrt{k_0^2\left(\varepsilon_{r\_layer} - 1\right) + k_{z\_air}^2} \tag{B6}$$

In these equations, k_{z_layer} are the z-directed wavenumbers; h_{layer} denotes the layer thickness and ε_{r_layer} the layer complex permittivity. The index "sub_layer" in Eq. (B5) indicates the layer under the considered layer (muscle for fat, fat for skin).

REFERENCES

1. Patel, M. and J. Wang, "Applications, challenges, and prospective in emerging body area networking technologies," *IEEE Wirel. Commun.*, Vol. 17, No. 1, 80–88, 2010.
2. Yuce, M. R. and J. Khan, *Wireless Body Area Networks: Technology, Implementation, and Applications*, CRC Press, 2011.
3. Li, H.-B. and K. Y. Yazdandoost, *Wireless Body Area Network*, River Publishers, 2010.
4. Zhu, N., "Simulation and optimization of energy consumption on wireless sensor networks," *Journal of the Institute of Polytechnics Osaka City University, Ser. A Mathematics*, Ecole Centrale de Lyon, 2013.

5. Aoyagi, T., M. Kim, and J. Takada, "Characterization for a electrically small antenna in proximity to human body — Towards Antenna de-embedding in body area network channel modeling," *7th European Conference on Antennas and Propagation*, 3421–3422, 2013.

6. Grimm, M. and D. Manteuffel, "On-Body antenna parameters," *IEEE Trans. Antennas Propag.*, Vol. 63, No. 12, 5812–5821, 2015.

7. Naganawa, J., J. Takada, T. Aoyagi, and M. Kim, "Antenna deembedding in WBAN channel modeling using spherical wave functions," *IEEE Trans. Antennas Propag.*, Vol. 65, No. 3, 1289–1300, 2017.

8. Boyes, S. J., P. J. Soh, Y. Huang, G. A. E. Vandenbosch, and N. Khiabani, "On-body performance of dual-band textile antennas," *IET Microwaves, Antennas Propag.*, Vol. 6, No. 15, 1696–1703, 2012.

9. Giddens, H., D. L. Paul, G. S. Hilton, and J. P. McGeehan, "Influence of body proximity on the efficiency of a wearable textile patch antenna," *6th European Conference on Antennas and Propagation (EuCAP)*, 1353–1357, 2012.

10. Klemm, M., I. Z. Kovacs, G. F. Pedersen, and G. Tröster, "Comparison of directional and omni-directional UWB antennas for Wireless Body Area Network applications," *18th Internaitonal Conference on Applied Electromagnetics and Communications (ICECom)*, 1–4, 2005.

11. Sarrazin, J., et al., "Antenna radiation efficiency considerations in body area networks," *11th EAI International Conference on Body Area Networks, ICST (Institute for Computer Sciences, Social-Informatics and Telecommunications Engineering)*, 10–11, 2016.

12. Razafimahatratra, S., J. Sarrazin, A. Benlarbi-delaï, and P. De Doncker, "Horn antenna design for BAN millimeter wave on-body communication," *IEEE APS*, 204.2, 2014.

13. Chahat, N., G. Valerio, M. Zhadobov, and R. Sauleau, "On-body propagation at 60 GHz," *IEEE Trans. Antennas Propag.*, Vol. 61, No. 4, 1876–1888, 2013.

14. Alipour, S., F. Parvaresh, H. Ghajari, and F. K. Donald, "Propagation characteristics for a 60 GHz Wireless Body Area Network (WBAN)," *Military Communications Conference*, 719–723, 2010.

15. Petrillo, L., T. Mavridis, J. Sarrazin, A. Benlarbi-Delai, and P. De Doncker, "Statistical on-body measurement results at 60 GHz," *IEEE Trans. Antennas Propag.*, Vol. 63, No. 1, 400–403, 2015.

16. Shubair, R. M. and Y. L. Chow, "A closed-form solution of vertical dipole antennas above a dielectric halfspace," *IEEE Trans. Antennas Propag.*, Vol. 41, No. 12, 1737–1741, 1993.

17. Hasgall, P. A., E. Neufeld, M. C. Gosselin, A. Klingenböck, and N. Kuster, "TIS database for thermal and electromagnetic, parameters of biological tissues," Version 2.6, 2015, [Online], Available: www.itis.ethz.ch/database.

18. Balanis, C. A., *Antenna Theory: Analysis and Design*, 3rd Edition, John Wiley and Sons, 2005.

19. Grimm, M. and D. Manteuffel, "Norton surface waves in the scope of body area networks," *IEEE Trans. Antennas Propag.*, Vol. 62, No. 5, 2616–2623, 2014.

20. King, R. W. P., G. J. Fikioris, and R. B. Mack, *Cylindrical Antennas and Arrays*, Cambridge University Press, 2002.

21. Lea, A., P. Hui, J. Ollikainen, and R. G. Vaughan, "Propagation between on-body antennas," *IEEE Trans. Antennas Propag.*, Vol. 57, No. 11, 3619–3627, 2009.

22. Alexander, H. and D. L. Miller, "Determining skin thickness with pulsed ultra sound," *Journal of Investigative Dermatology*, Vol. 72, No. 1, 17–19, 1979.

23. Marks, R., P. J. Dykes, and E. Roberts, "The measurement of corticosteroid induced dermal atrophy by a radiological method," *Archives of Dermatological Research*, Vol. 253, No. 2, 93–96, Sep. 1975.

24. Shelkunoff, H. T. and S. A. Friis, *Antennas: Theory and Practice*, Wiley, New York, 1952.

25. Compton, R. T., "The admittance of aperture antennas radiating into lossy media," Antenna Lab., The Ohio State University Research Foundation, Columbus, Rept. 1691-5, Mar. 15, 1964.

26. Yang, J. J., Y. L. Chow, and D. G. Fang, "Discrete complex images of a three-dimensional dipole above and within a lossy ground," *IEE Proc. H (Microwaves, Antennas Propagation), IET Digit. Libr.*, Vol. 138, No. 4, 319–326, 1991.

27. Xu, X. and Y. F. Huang, "An efficient analysis of vertical dipole antennas above a lossy half-space," *Progress In Electromagnetics Research*, Vol. 74, 353–377, 2007.

28. Khalatpour, A., R. Sarraf Shirazi, and G. Moradi, "Analysis of vertical wire antennas above lossy half-space using matrix pencil method," *AEU — Int. J. Electron. Commun.*, Vol. 64, No. 8, 784–789, 2010.

29. Shubair, R. M. and Y. L. Chow, "A simple and accurate complex image interpretation of vertical antennas present in contiguous dielectric half-spaces," *IEEE Trans. Antennas Propag.*, Vol. 41, No. 6, 1993.

30. Michalski, K. A. and J. R. Mosig, "The Sommerfeld half-space problem revisited: From radio frequencies and Zenneck waves to visible light and Fano modes," *Journal of Electromagnetic Waves and Applications*, Vol. 30, No. 1, 1-42, 2016.

31. Felsen, L. and N. Marcuvitz, *Radiation and Scattering of Waves*, Prentice-Hall, 1973.

32. Ur-Rehman, M., N. A. Malik, X. Yang, Q. H. Abbasi, Z. Zhang, and N. Zhao, "A low profile antenna for millimeter-wave body-centric applications," *IEEE Trans. Antennas Propag.*, Vol. PP, No. 99, 1-1, 2017.

33. Puskely, J., M. Pokorny, J. Lacik, and Z. Raida, "Antenna implementable into button for on-body communications at 61 GHz," *8th European Conference on Antennas and Propagation (EuCAP)*, 1551–1555, 2014.